Citalopram exhibits immune-dependent anti-tumor effects by modulating C5aR1^{+} TAMs

Fangyuan Dong[1, 8], Shan Zhang[2, 8], Kaiyuan Song[3, 8], Luju Jiang[2, 8], Li-Peng Hu[2], Qing Li[2], Xue-Li Zhang[2], Jun Li[2], Mingxuan Feng[4], Zhi-Wei Cai[5], Hong-Fei Yao[5], Rong-Kun Li[6], Hui Li[2], Jie Chen[1], Xiaona Hu[1], Jiaofeng Wang[1], Chongyi Jiang[5], Helen He Zhu[7], Cun Wang[2], Lin-Tai Da[3], Zhi-Gang Zhang[2, #], Zhijun Bao[1, #], Xu Wang[6, #], Shu-Heng Jiang[2, #]

[1]Department of Gastroenterology, Shanghai Key Laboratory of Clinical Geriatric Medicine, Shanghai Institute of Geriatrics and Gerontology, Huadong Hospital, Fudan University, Shanghai 200040, P.R. China;

[2]State Key Laboratory of Systems Medicine for Cancer, Shanghai Cancer Institute, Ren Ji Hospital, School of Medicine, Shanghai Jiao Tong University, Shanghai 200240, P.R. China;

[3]Key Laboratory of Systems Biomedicine (Ministry of Education), Shanghai Center for Systems Biomedicine, Shanghai Jiao Tong University, Shanghai 200240, P.R. China;

[4]Department of Liver Surgery, Ren Ji Hospital, School of Medicine, Shanghai Jiao Tong University, Shanghai 200127, P.R. China;

[5]Department of General Surgery, Hepato-biliary-pancreatic Center, Huadong Hospital, Fudan University, Shanghai 200040, P.R. China;

[6]Institute of Oncology, Affiliated Hospital of Jiangsu University, Zhenjiang 212001, P.R. China;

[7]State Key Laboratory of Systems Medicine for Cancer, Renji-Med-X Stem Cell Research Center, Shanghai Cancer Institute & Department of Urology, Ren Ji Hospital, Shanghai Jiao Tong University School of Medicine, Shanghai, 200127, P.R. China.

[8]These authors contributed equally to this work

[#]Correspondence

zzhang@shsci.org (Z.G.Z); zhijunbao@fudan.edu.cn (Z.B.); wangxu@ujs.edu.cn (X.W.); shjiang@shsci.org (S.H.J.).

Abstract

Administration of selective serotonin reuptake inhibitors (SSRIs) is associated with a reduced cancer risk and shows significant anti-tumor effects across multiple tumor types, suggesting the potential for repurposing SSRIs in cancer therapy. Nonetheless, the specific molecular target and mechanism of action of SSRIs remain to be fully elucidated. Here, we reveal that citalopram exerts an immune-dependent anti-tumor effects in hepatocellular carcinoma (HCC). Interestingly, the anti-HCC effects of citalopram are not reliant on its conventional target, the serotonin transporter. Through various drug repurposing approaches, including global reverse gene expression profiling, drug affinity responsive target stability assay, and molecular docking, the complement component 5a receptor 1 (C5aR1) is identified as a new target of citalopram. C5aR1 is predominantly expressed by tumor-associated macrophages (TAMs), and citalopram treatment enhances local macrophage phagocytosis and elicits $CD8^+$ T anti-tumor immunity. C5aR1 deficiency or depletion of $CD8^+$ T cells hinders the anti-HCC effects of citalopram. Collectively, our study reveals the immunomodulatory roles of citalopram in inducing anti-tumor immunity, and provides a basis for considering the repurposing of SSRIs as promising anticancer agents for HCC treatment.

Key words: Drug repurposing, Drug discovery, SLC6A4, SERT, 5-HT

Introduction

The development of anti-tumor drugs encounters numerous challenges, such as a high failure rate, substantial costs, limited bioavailability, safety concerns, and lengthy design and testing procedures (Pushpakom, Iorio et al., 2019). As different diseases may share common pathological mechanisms, there is a growing focus on repurposing existing drugs for new applications, referred to as “new uses for old drugs” (Foretz, Guigas et al., 2023, Schipper, Zeverijn et al., 2022). Additionally, exploring new disease-relevant targets for established drugs and broadening their indications offers significant translational value (Xia, Sun et al., 2024).

Selective serotonin reuptake inhibitors (SSRIs; i.e., citalopram, escitalopram, fluoxetine, fluvoxamine, paroxetine, and sertraline) are frequently prescribed to treat conditions such as depression, anxiety, insomnia, and chronic pain (Fluyau, Mitra et al., 2022). SSRIs target the serotonin transporter (SERT, encoded by the *SLC6A4* gene), blocking the reuptake of serotonin (5-hydroxytryptamine, 5-HT) into the presynaptic neuron, ultimately increasing 5-HT levels in the brain (Singh, Seth et al., 2023). Recent population-based epidemiological studies suggest that SSRIs have the potential to reduce the risk of many cancers, including kidney, breast, colorectal, and liver cancers (Bhagavathula, Woolf et al., 2022, Fischer, Rennert et al., 2022, Lee, Huang et al., 2021, Zhang, Sundquist et al., 2021). The anxiety and depression symptoms among cancer patients is increasingly recognized (Carlson, Ismaila et al., 2023). Considering the established safety profile and known side effects of SSRIs, repurposing these drugs as potential anti-tumor agents, particularly for cancer patients with comorbid depression, could offer dual benefits. This approach may not only help improve neurological function but also potentially impede tumor progression. Hence, repurposing SSRIs could present a cost-effective option. Nevertheless, the mechanisms of actions responsible for the anti-tumor effects of SSRIs are still largely unknown.

In this study, using hepatocellular carcinoma (HCC) as a model, we revealed that citalopram, an SSRI, exhibits anti-tumor properties not through its traditional target SERT, but instead via partially immune-dependent mechanisms. Through a comprehensive approach involving global reverse gene expression profiling, drug affinity responsive target stability (DARTS) (Lomenick, Hao et al., 2009), and molecular docking analyses, we identified the

complement component 5a receptor 1 (C5aR1), predominantly expressed by tumor-associated macrophages (TAMs), as a target of citalopram. C5aR1 play critical roles in fostering an immunosuppressive microenvironment (Beach, MacLean et al., 2023, Medler, Murugan et al., 2018) and boosting the metastatic potential of cancer cells (Ajona, Zandueta et al., 2018). Targeting C5aR1^{+} TAMs effectively reverses tumor progression and enhances anti-tumor response (Li, Poire et al., 2024, Luan, Lei et al., 2024, Zhao, Yao et al., 2024). Given its significant impact on cancer progression, C5aR1 has surfaced as a promising therapeutic target for potential cancer interventions. Here, we further elucidated the mechanism underlying the connection between C5aR1^{+} TAMs and citalopram-related phenotypes.

Results

The immune-dependent anti-tumor effects of citalopram in HCC

Previously, we have demonstrated the direct effects of citalopram on cancer cell proliferation, apoptosis, and metabolic processes (Dong, He et al., 2024). To further evaluate the therapeutic effects of citalopram, we engrafted mouse Hepa1-6 and Hep53.4 cells into different strains of recipient mice, including the immune-competent C57BL/6 mice and immune-compromised *Rag1*$^{-/-}$ mice. Citalopram was given by i.p. administration daily for 15-25 days after bearing palpable tumors (~50 mm^3). Tumor growth was significantly retarded in both two mouse models. Of note, this impairment was more pronounced in immune-competent C57BL/6 mice (**Figures 1A-B**), indicating an immune-dependent effect of citalopram, although the possibility of other non-immune mechanisms remains. This finding was further validated at molecular levels, as evidenced by reduced staining of the proliferation index Ki67 and increased expression of cleaved caspase 3 (CCS3) (**Figure S1**).

As SERT is the known target of SSRIs, we tested the therapeutic effect of citalopram in the absence of SERT (**Figures 1C-D**). In mouse HCC cells, SERT knockdown did not significantly impact cell proliferation or apoptosis, both *in vitro* and *in vivo* (**Figures 1E-F and S2A-B**). However, citalopram delayed the growth of SERT-silenced HCC tumors, and its suppressive effect was more proficient in immune-competent hosts compared with *Rag1*$^{-/-}$ ones (**Figures 1E-F and S2C-F**). Together, these data suggest that citalopram might target

other molecules instead of SERT to exhibit an immune-dependent anti-tumor effects in HCC. Using a single cell sequencing dataset of HCC (GSE125449), we revealed that SERT is expressed not only in HCC cells but also in T cells, tumor-associated endothelial cells, and cancer-associated fibroblasts (**Figure S2G**). Therefore, we cannot fully rule out the possibility that citalopram may influence these cellular components within the tumor microenvironment (TME) and contribute to its therapeutic effects.

C5aR1 is a direct target of citalopram

Previously, using drug-induced gene signature networks and target prediction method, we identified a repertoire of targets related to citalopram treatment (Dong et al., 2024). The top two hits are glucose transporter 1 (GLUT1) and C5aR1 (**Figures 2A-B**). Citalopram can reverse the Warburg effect to inhibit HCC by targeting GLUT1 directly (Dong et al., 2024). Considering the significant role of C5aR1 in immune modulation (Pio, Ajona et al., 2019), we investigated whether the immune-dependent anti-tumor effects of citalopram are mediated through C5aR1. Immunohistochemical analysis showed that the positive staining of C5aR1 was predominantly found in scattered immune cells (**Figure 2C**). Single-cell sequencing data indicated that C5aR1 was expressed at higher levels in monocytes/macrophages within the TME compared with other cell types (**Figure 2D**). Co-immunofluorescence analysis corroborated that $CD163^{+}$ macrophages presented significant C5aR1 immunoreactivity (**Figure 2E**). As previously reported (Zhang, He et al., 2019), six distinct macrophage subclusters have been identified in HCC, with M4-c1-THBS1 and M4-c2-C1QA demonstrating significant enrichment in tumor tissues. The M4-c1-THBS1 cluster is associated with signatures characteristic of myeloid-derived suppressor cells (MDSCs), whereas the M4-c2-C1QA cluster displays features resembling those of TAMs as well as M1 and M2 macrophages. We found that C5aR1 is highly expressed in these two clusters, while the expression levels in the other macrophage clusters were considerably lower (**Figure S3**).

The DARTS assay is widely recognized technique used to identify potential protein targets for small molecules. This approach involves conferring proteolytic protection of target proteins by their interaction with small molecules. Combined DARTS assay with immunoblotting analysis, we investigated the stability of C5aR1 against pronase in the

presence or absence of citalopram treatment. Because C5aR1 is expressed by macrophages, THP-1 cells were employed for the DARTS assay. Citalopram did not affect the basal protein level of C5aR1 in macrophages (**Figure 2F**). However, citalopram could enhance the stability of C5aR1 against pronase treatment. Of note, this effect was specific to C5aR1, as citalopram did not impact the proteolytic susceptibility of β-actin (**Figure 2F**). Moreover, the stability of C5aR1 against pronase was enhanced in a dose-dependent manner following treatment with citalopram (**Figure 2G**). Besides citalopram, other 5 SSRIs (escitalopram, fluoxetine, fluvoxamine, paroxetine, and sertraline) also played protective roles of C5aR1 against pronase (**Figure S4A**).

To address citalopram/C5aR1 interaction, *in silico* docking analysis was conducted. Previous studies revealed two different inhibitor-binding sites in C5aR1, namely, the orthosteric site on the extracellular side and the allosteric site outside the transmembrane bundle (Robertson, Rappas et al., 2018). Therefore, we docked the structure of citalopram into both orthosteric and allosteric sites of human C5aR1 (PDB id: 6C1Q), respectively. *In silico* docking of citalopram into the orthosteric site predicted two binding conformations without overlap (**Figures 2H and S4B**). In pose-1, the fluorophenyl and the cyanophtalane group of citalopram stacked with the side chains of Y258 and R206, and the amino group of citalopram interacted with the negatively charged residue E199 (**Figure 2I**, left). In pose-2, two negatively charged residues, D282 and D37, surrounded the amino group (**Figure 2I**, middle). Considering the accessibility, D282 orienting towards the binding cavity of C5aR1 might play a more pivotal role in the citalopram binding event proposed by pose-2. Additionally, the cyanophtalane group of citalopram interacted with hydrophobic residues L92 and P113 of C5aR1. The fluorine was inserted into a narrow space lying over the side chain of W102 (**Figure 2I**, right). For the allosteric site, residue W213 played a critical role in inhibitor binding via hydrogen-bond interactions established by the amino group in the indole ring (Liu, Kim et al., 2018). According to the best pose from cluster 2, the citalopram formed a hydrogen-bond via the oxygen atom in the cyanophtalane group with W213 (**Figure 2I**, right). Inspired by these molecular docking results, we generated six C5aR1 mutants to figure out the real binding site of citalopram in HEK293T cells (**Figure S4C**). Indeed, citalopram had no protective effects on C5aR1 stability with the transfection of HA-C5aR1 E199 and D282

mutant against pronase (**Figure 2J**). Consistently, mutations on E199 and D282 reduce C5a binding affinity to C5aR1 (Wang, Liu et al., 2023). Furthermore, docking analysis and DARTS assay revealed that other four SSRIs could bind to the D282 site of C5aR1 (**Figures S4D-E**). These findings demonstrate that SSRIs adopt the orthosteric site to bind to C5aR1 and electrostatic interactions between C5aR1 D282 and the amino groups of SSRIs play an instrumental role in the binding mechanisms.

Citalopram targets C5aR1 in TAMs

C5aR1, the receptor for anaphylatoxin C5a, is profoundly implicated in tumor progression via inducing an immunosuppressive microenvironment in which TAMs are involved (Medler et al., 2018). As C5aR1 is localized in TAMs within the TME of HCC, we explored whether citalopram exerted anti-tumor functions by targeting C5aR1 on TAMs. Given that citalopram also targets GLUT1 in HCC (Dong et al., 2024), we generated a Hepa1-6 clone with complete knockdown of GLUT1 ($GLUT1^{KD}$) to dissect C5aR1-dependent roles (**Figure 3A**). Interestingly, citalopram displayed an inhibitory effect on $GLUT1^{KD}$ tumors in immune-component C57BL/6 mice but not *Rag1*$^{-/-}$ ones (**Figure 3B**), underscoring the contribution of C5aR1. To delineate the involvement of macrophages, we first depleted mouse macrophages with clodro-Liposomes and found that citalopram was ineffective in controlling $GLUT1^{KD}$ tumors (**Figure S5**), implying the influences of citalopram on macrophages. As the second line of evidence, we engrafted $GLUT1^{KD}$ Hepa1-6 cells into the syngeneic *C5ar*1$^{+/-}$ and *C5ar*1$^{-/-}$ mice. Compared with *C5ar1*$^{+/-}$ recipients, tumor growth was attenuated in *C5ar1*$^{-/-}$ recipients (**Figure 3C**), whereas C5a deposition remained unchanged (**Figure 3D**), suggesting that while C5a is still present, its interaction with C5aR1 is critical for influencing tumor growth dynamics. Third, we injected $GLUT1^{KD}$ Hepa1-6 cells into syngeneic recipient *C5ar1*$^{-/-}$ (r*C5ar1*$^{-/-}$) mice that had been reconstituted with donor *C5ar1*$^{+/-}$ (d*C5ar1*$^{+/-}$) or *C5ar1*$^{-/-}$ (d*C5ar1*$^{-/-}$) bone marrow (BM) cells to analyze the therapeutic effect of citalopram (**Figure 3E**). Implantation of donor *C5ar1*$^{+/-}$ BM into *C5ar1*$^{-/-}$ recipients restored tumor growth compared with their *C5ar1*$^{-/-}$ counterparts and citalopram cannot restrict tumor growth in r*C5ar1*$^{-/-}$; d*C5ar1*$^{-/-}$ mice; in contrast, tumor growth kinetics were considerably diminished in r*C5ar1*$^{-/-}$; d*C5ar1*$^{+/-}$ mice upon citalopram treatment (**Figure 3F**), suggesting that $C5aR1^{+}$ TAM rewiring

enables the tumoricidal effects of citalopram. Notably, citalopram treatment did not affect C5a deposition (**Figure 3G**), highlighting that the impact of citalopram is primarily on C5a/C5aR1 interactions and downstream signaling pathways, rather than on altering C5a levels.

To answer how C5aR1^{+} macrophages mediate citalopram-induced anti-tumor effects, we probed macrophage functions. Given the crucial role of the C5a/C5aR1 axis in macrophage phagocytosis (Wang, Liang et al., 2023), we investigated whether citalopram has an effect on this process. Phagocytosis assay showed that isolated TAMs from *C5ar1*$^{-/-}$ recipients had higher phagocytic capacity of HCC cells than that of *C5ar1*$^{+/-}$ recipients (**Figure 3H**). Consistently, GSEA indicated a significant enrichment of the phagocytosis pathway in macrophages derived from *C5ar1*$^{-/-}$ mice compared to those from *C5ar1*$^{+/-}$ mice (**Figure S6A**). Moreover, citalopram increased the phagocytosis of TAMs from r*C5ar1*$^{-/-}$; d*C5ar1*$^{+/-}$ mice (**Figure 3I**). C5a-mediated macrophage phagocytic impairment was reversed by C5aR1 knockdown or treatment with citalopram or different SSRIs (**Figures S6B-D**). C5a was able to suppress, while citalopram was effective in bolstering phagocytosis in macrophages expressing C5aR1^{WT} but not C5aR1^{D282A} (**Figures S6E-F**). Despite several residues of mouse C5aR1 protein being different from that of human C5aR1, citalopram shared a similar binding model with them (**Figure S7**). Given citalopram's reported role in inhibiting GLUT1, we tested whether citalopram affects macrophage metabolism. However, the glycolytic metabolism of THP-1 cells remained largely unaffected following citalopram treatment, as evidenced by glucose uptake, lactate release, and extracellular acidification rate (ECAR) (**Figure S8A**). Next, we mined a single cell sequencing datasets of HCC and revealed that TAMs predominantly express GLUT3 but not GLUT1 (**Figure S8B**). Consistently, Western blotting analysis showed a higher expression of GLUT3 and minimal levels of GLUT1 in THP-1 cells (**Figure S8C**). GLUT1 knockdown in THP-1 cells did not significantly affect their glycolytic metabolism, whereas GLUT3 knockdown led to a marked reduction in glycolysis in THP-1 cells (**Figures S8C-D**). Therefore, the effects of citalopram on macrophages might be primarily mediated through targeting C5aR1 rather than GLUT1.

In orthotopic GLUT1^{KD} Hepa1-6 models, flow cytometry revealed a significant reduction of TAMs in the citalopram group compared with the control group (**Figure 3J**). Moreover, TAM polarization was shifted to a proinflammatory state, as evidenced by flow cytometry (**Figure**

3K) and real-time qPCR analysis (**Figure S9A**). Further phenotyping of tumor immune subsets in immunocompetent C57BL/6 mice showed that citalopram increased the infiltration of $CD8^+$ T and dendritic cells while decreasing the infiltration of $CD4^+$ T and $B220^+$ B cells (**Figures 3L and S9B-C**). No significant changes were observed in splenic immune subsets upon citalopram treatment (**Figure S9D**).

Next, we sought to understand whether $C5aR1^+$ TAMs impact on $CD8^+$ T cells. Intratumoral $CD8^+$ T cells from tumor-bearing *C5ar1*$^{-/-}$ mice had increased frequency and expression of GZMB, IFN-γ, and TNF-α compared with that from *C5ar1*$^{+/-}$ mice (**Figure 3M**). Likewise, the frequency and cytotoxicity of $CD8^+$ T cell from r*C5ar1*$^{-/-}$; d*C5ar1*$^{+/-}$ mice were reduced compared with r*C5ar1*$^{-/-}$; d*C5ar1*$^{-/-}$ mice, and this effect was partially reversed by citalopram treatment (**Figure 3N**). Furthermore, depletion of $CD8^+$ T cells abrogated the $C5aR1^+$ TAM-mediated enhancement of tumor growth (**Figure 3O**), suggesting that the anti-tumor effects of $CD8^+$ T cells are required for the pro-tumor phenotype of $C5aR1^+$ TAMs. Clinically, data from TCGA cohort reinforced the link between C5aR1 expression and an immunosuppressive TME as demonstrated by the associations with TAMs, exhausted T cells, immune checkpoint molecules, and effector Tregs (**Figure 3P**).

Citalopram and $CD8^+$ T cell activation

Considering the fact that citalopram targets GLUT1 and $CD8^+$ T cell function is reliant on glycolytic metabolism (Cao, Liao et al., 2023, Dong et al., 2024), we investigated the *in vivo* effects of citalopram on $CD8^+$ T cells. Citalopram significantly invigorated $CD8^+$ T cell function and glycolytic metabolism in intrahepatic tumors from WT C57BL/6 mice (**Figures 4A-B**). To simulate the role of metabolic-associated fatty liver disease (MAFLD) in the development of cirrhosis and HCC (Du, Liu et al., 2022, Eslam, Newsome et al., 2020), we fed C57BL/6 mice a choline-deficient, amino acid-defined high-fat diet (CDAHFD) to induce metabolic dysfunction-associated steatohepatitis (MASH)/fibrosis prior to orthotopic Hepa1-6 cell implantation. Likewise, $CD8^+$ T cell function and glycolytic metabolism were enhanced by citalopram treatment in MASH mice (**Figures 4C-D**). GLUT1-deficient cytotoxic T cells remain phenotypically and functionally unaffected (Macintyre, Gerriets et al., 2014), indicating that other glucose uptake mechanisms exist in cytotoxic T cells. GLUT1 and GLUT3 are essential

for the activation and effector function of T cells (Hochrein, Wu et al., 2022, Macintyre et al., 2014). Similar to TAMs, intratumoral $CD8^+$ T cells massively upregulated GLUT3 but not GLUT1 (**Figure S9E**), and this finding was supported by single cell sequencing analysis (**Figure S8B**), suggesting the GLUT3-dependent glucose uptake in $CD8^+$ T cells.

Given the wide range of peripheral 5-HT actions (Jiang, Wang et al., 2021), we hypothesized that citalopram modulates the immune system through the serotonergic mechanisms. Indeed, citalopram administered for 2 weeks in tumor-bearing mice led to reduced serum 5-HT levels (**Figure 4E**), which were accompanied with a reduction of low-grade systemic inflammatory responses in the MASH mice (**Figure 4F**). Compared to the control C57BL/6 mice, tumor-bearing *Tph1*$^{-/-}$ mice, which lack peripheral 5-HT, exhibited slowed tumor growth and increased effector function of intratumoral $CD8^+$ T cells (**Figures 4G-I**). Interestingly, citalopram reduced serum 5-HT to a level as observed in *Tph1*$^{-/-}$ mice, and displayed a superior inhibitory effect on tumor growth and $CD8^+$ T cell function compared with that induced by *Tph1* deficiency (**Figures 4G-I**). These data not only corroborate recent reports that SSRIs modulate $CD8^+$ T cell function via serotonergic-dependent mechanism (Li, Elsten-Brown et al., 2025), but also reveals additional *in vivo* regulatory avenues by which citalopram affects $CD8^+$ T cells, such as its ability to reprogram $C5aR1^+$ TAMs. Notably, in the context of macrophage depletion, $CD8^+$ T cell cytotoxicity was not further enhanced by citalopram (**Figure S5E**), indicating that TAM-dependent pathways are central to $CD8^+$ T cell-mediated anti-tumor immunity and largely underlie the anti-tumor effects of citalopram.

Next, we investigated the direct effects of citalopram on T cell activation, expansion, and cytotoxicity. Citalopram enhanced αCD3/αCD28-stimulated $CD8^+$ T cell proliferation as indicated by CFSE staining (**Figure S10A**). Moreover, citalopram promoted the TCR-instigated activation of $CD8^+$ T cells and the generation of effector $CD8^+$ T cells as evidenced by the cell surface expression of CD44 and CD62L (**Figure S10B**). Likewise, the cytotoxic activity of activated $CD8^+$ T was enhanced by citalopram, as reflected by GZMB, IFNγ, and TNF-α staining (**Figures S10C-E**).

Finally, to examine the immune-dependent anti-tumor effects of citalopram, we depleted either $CD8^+$ or $CD4^+$ T cells from $GLUT1^{KD}$ Hepa1-6 tumor-bearing mice and found that depletion of $CD8^+$ T cells, rather than $CD4^+$ T cells, increased tumor growth in citalopram-

treated mice but had marginal effects in control mice (**Figure 4J**), showing that $CD8^+$ T cells are essential for the effector mechanisms of citalopram.

Discussion

Repurposing approved non-oncology drugs for cancer therapy offers cost-effectiveness, an accelerated development timeline, and a known safety profile as key advantages. Accumulating studies have deciphered the inverse link between SSRIs use and cancer risk. However, there is a scarcity of studies investigating the potential repurposing SSRIs for cancer treatment and their mechanisms of action. Non-oncology drugs may have mechanisms of action that are different from traditional cancer treatments. Previously, we and others have uncovered several new targets of SSRIs, including GLUT1 in HCC (Dong et al., 2024), SMPD1 in glioblastoma (Bi, Khan et al., 2021), and VDAC1 in autophagy (Hwang, Shim et al., 2021). Here, we further broaden the knowledge of how SSRIs impact the immune system to exert anti-tumor effects. By targeting C5aR1 on TAMs, citalopram enhances the phagocytic activity of TAMs and boosts local anti-tumor immune responses, particularly $CD8^+$ T cell anti-tumor immunity. Furthermore, citalopram has a direct stimulatory effect on the activation of $CD8^+$ T cells *in vitro* (**Figure 5**).

C5aR1 is expressed on TAMs within the TME, which helps to explain why citalopram has better anti-tumor effects in immune-competent mice. In addition to TAMs, C5aR1 is also expressed by neutrophils, mast cells, and myeloid-derived suppressor cells in cancers (Ding, Li et al., 2020, Medler et al., 2018, Ou, Liu et al., 2021). Although the functional impacts of citalopram on these C5aR1-expressing immune cells have not been formally determined, macrophage depletion assay and $C5aR1^{-/-}$ BM transfer experiment suggested that citalopram exerted anti-tumor functions *in vivo* through C5aR1-expressing TAMs. Targeting C5aR1 can reprogram TAMs from a protumor state to an antitumor state, promoting the secretion of CXCL9 and CXCL10 while facilitating the recruitment of cytotoxic $CD8^+$ T cells (Luan et al., 2024, Medler et al., 2018). In alignment with this, citalopram treatment increased $CD8^+$ T cell filtration and their cytotoxic activities in HCC, and this effect was largely dependent on $C5aR1^+$ macrophages. Citalopram induces TAM phenotypic polarization towards to a M1 proinflammatory state (Zhao et al., 2024), which supports anti-tumor immune response within

the TME. Another possibility is that citalopram targets C5aR1 to enhance macrophage phagocytosis and subsequent antigen presentation and/or cytokine production, which promotes T cell recruitment and activity as well as modulate other aspects of tumor immunity. Therefore, we provide a mechanistic insight regarding how citalopram target C5aR1 activity in TAMs, the central findings are important to our understanding of citalopram-induced anti-tumor activities and may lay a basis for upcoming mechanistic studies aimed to decipher specific tumor-promoting roles of this defined TAM population.

While we highlight the anti-HCC effects of SSRIs through targeting C5aR1, it is possible that SSRIs impact tumor progression by modulating the systemic environment via serotonergic mechanisms, especially concerning the activation of $CD8^+$ T cells. Apart from its role in regulating hemostasis, 5-HT exerts immunoregulatory functions on circulating immune cells (Costa, Santos et al., 2020). In this study, it was observed that both citalopram treatment and *Tph1* deficiency enhanced $CD8^+$ T cell cytotoxic activity. Peripheral 5-HT has been shown to enhance PD-L1 expression on cancer cells, thereby impairing functions of $CD8^+$ T cells within tumors (Schneider, Heeb et al., 2021). 5-HT deficiency delays the growth of syngeneic pancreatic and colorectal tumors by promoting the accumulation and effector functions of $CD8^+$ T cells (Schneider et al., 2021). In addition to the traditional receptor-dependent signaling transduction, 5-HT can modulate $CD8^+$ T activity through post-translational modification known as serotonylation (Wang, Fu et al., 2024). $CD8^+$ T cells express TPH1 (Li et al., 2025, Wang et al., 2024), enabling them to synthesize endogenous 5-HT, which activates their activity through serotonylation-dependent mechanisms. It remains to be explored whether serotonylation contributes to the immunomodulatory effects of citalopram, as citalopram directly stimulates $CD8^+$ T cell proliferation, activation, and cytotoxicity *in vitro*. The observed reduction in serum 5-HT levels and activation of $CD8^+$ T cells following SSRI treatment further highlight the complex interplay between neurotransmitters, the immune system, and cancer progression. Although citalopram directly stimulates $CD8^+$ T cells *in vitro*, the TAM-independent activation is not evident *in vivo* within the complex TME, as $CD8^+$ T cell responses are abolished by macrophage depletion, indicating that the *in vivo* effects of citalopram on $CD8^+$ T cells and tumor growth are largely TAM-dependent.

Citalopram docks into the GLUT1 pocket with an electrostatic contact to E380 and

surrounding hydrophobic contacts (Dong et al., 2024). Although GLUT1 and GLUT3 share a highly conserved core substrate-binding pocket, isoform-specific regulation arises from features outside the canonical site. Structural homology between GLUT1 and GLUT3 is high in the transmembrane core, but regulatory features, such as the cytosolic Sugar Porter (SP) motif network, the conserved A motif, lipid interfaces, and gating dynamics, differ between the two isoforms (Custódio, Paulsen et al., 2021). These differences can alter pocket accessibility, coupling to conformational transitions, and allosteric signaling to the cytosol, such that a GLUT1 inward-facing binder may not stabilize a GLUT3 conformation that yields appreciable transport inhibition. Consistently, functional experiments show robust GLUT1 engagement in cancer cells (Dong et al., 2024), while equivalent GLUT3 inhibition has not been observed in TAMs (**Figure S8**), supporting isoform-selective targeting by citalopram in this context.

In a study involving 308,938 participants with HCC, findings indicated that the use of antidepressants following an HCC diagnosis was linked to a decreased risk of both overall mortality and cancer-specific mortality (Huang, Chen et al., 2023). These associations were consistently observed across various subgroups, including different classes of antidepressants and patients with comorbidities such as hepatitis B or C infections, liver cirrhosis, and alcohol use disorders (Huang et al., 2023). Similarly, our analysis of real-world data from the Swedish Cancer Register demonstrated that SSRIs are correlated with slower disease progression in HCC patients (Dong et al., 2024). Given these insights, antidepressants, especially SSRIs, show significant potential as anticancer therapies for individuals diagnosed with HCC. Immunotherapy, especially immune checkpoint inhibitors (ICIs), has revolutionized the management of HCC (Zheng, Wang et al., 2021). The immune microenvironments play crucial roles in the response or resistance of HCC to immunotherapies (Llovet, Castet et al., 2022). However, limited molecular biomarkers are available to guide clinical decision-making for ICI therapy of HCC. Given SSRIs can increase $CD8^+$ T cell infiltration as well as cytotoxic activities by targeting $C5aR1^+$ TAMs, one can suppose that $C5aR1^+$ TAMs within the HCC microenvironment might be used as a molecular marker for SSRIs use in combination with ICI therapy.

There are several limitations in this study. First, the potential promiscuity of citalopram's interactions across GLUT1, C5aR1, and SERT1, as varying affinities could influence the

drug's overall efficacy. Citalopram interacts with C5aR1 and GLUT1 through distinct binding sites and mechanisms, as whereas its interaction with SERT is characterized by a more direct inhibition of serotonin binding (Coleman, Green et al., 2016). Employing techniques such as surface plasmon resonance or biolayer interferometry could provide valuable quantitative data on binding kinetics and affinities for each target. Second, it is challenging to dissect how citalopram's interactions with multiple targets may contribute to its therapeutic effects, particularly in the context of immune modulation and tumor progression. The potential for citalopram to exhibit diverse mechanisms of action through these interactions warrants further investigation.

In conclusion, our study suggests the potential repurposing of SSRIs for the treatment of HCC and highlights C5aR1 as a direct target of citalopram. Citalopram exerts its effects through an immune-mediated pathway, primarily by targeting C5aR1^{+} TAMs. Combining SSRIs with ICIs or other first-line therapies could enhance the treatment efficacy of current standard therapies.

Materials and Methods

Animal models

In the subcutaneous xenograft model, *Rag1*$^{-/-}$ C57BL/6 mice (male, 6-8-week-old, Cyagen Biosciences, C001197), wild type immune-competent C57BL/6 mice (male or female, 6-8-week-old) or *Tph1*$^{-/-}$ mice (male, 6-8-week-old, Cyagen Biosciences, S-KO-05541), were maintained on a 12-hour day/night cycle with ad libitum access to food and water. For the pharmacological inhibition study, 5 × 10^6 mouse HCC cells (wild type, shControl, sh*Slc6a4* or sh*Slc2a1* Hepa1-6 and Hep53.4) in 100 μl PBS were injected subcutaneously in the lower back. When bore visible tumors, mice were given intraperitoneal injections of vehicle or citalopram (5 mg/kg body weight, Selleck, Shanghai, China) daily (n = 5-7 per group).

In the orthotopic xenograft model, 5 × 10^6 Hepa1-6 cells transfected with luciferase-expressing lentiviruses were orthotopically implanted into the liver of WT or MASH C57BL/6 mice. The day following tumor cell implantation, mice were treated with citalopram (5 mg/kg body weight) or DMSO. In the diet-induced MASH model, mice were fed a choline-deficient, amino acid-defined high-fat diet (45 kcal% fat) supplemented with 0.1% methionine (CDAHFD

diet, A06071309, from Research Diets) for a duration of 6 weeks.

For the C5aR1 knockdown study, C57BL/6J-*C5ar1*^{em1Cya} mice were purchased from Cyagen Biosciences (S-KO-01274, Suzhou, China). 5 × 10^6 sh*Slc2a1* Hepa1-6 cells were injected into the lower back of 6-8-week-old male *C5ar1*$^{+/-}$ or *C5ar1*$^{-/-}$ C57BL/6 mice. Tumor volume was measured every week using a digital caliper. Four weeks later, mice were sacrificed and xenograft tumors were analyzed.

To determine the association between citalopram and C5aR1, bone marrow transfer experiments were performed. Six- to eight-week-old male *C5ar1*$^{-/-}$ C57BL/6 mice were served as recipients. Mice underwent full-body irradiation for conditioning. Bone marrow was harvested from the femurs and tibias of donor mice carrying C5ar1 genotypes *C5ar1*$^{+/-}$ or *C5ar1*$^{-/-}$), and 1.0 × 10^7 cells were delivered intravenously into each recipient. After transplantation, mice were given antibiotic-supplemented water for 4 weeks to support engraftment. Ten weeks post-transplant, the recipients were considered fully immune-reconstituted and were used for GLUT1^{KO} Hepa1-6 tumor challenge experiments. A total of 2 × 10^6 GLUT1^{KO} Hepa1-6 cells were injected subcutaneously into the lower back of each recipient. One week after cancer cell implantation, mice were subjected to treatment with citalopram (5 mg/kg body weight) or DMSO. At indicated time point, mice were sacrificed and xenograft tumors were analyzed.

In all animal studies, tumor volume was assessed using caliper measurements and calculated using the formula: tumor = 1/2(length × width^2), where length represents the largest diameter and width indicates the smallest diameter. At the experimental endpoint, mice were humanely euthanized, tumors were excised, and tumor weight was recorded. All animals received proper care in accordance with the guidelines outlined in the “Guide for the Care and Use of Laboratory Animals” established by the National Academy of Sciences and published by the National Institutes of Health (NIH publication 86-23 revised 1985). The protocols for animal studies were approved by the ethics committee of the Ren Ji Hospital, School of Medicine, Shanghai Jiao Tong University (approval number 202201427 and RA-2021-096).

Cell culture and reagents

The following cell lines were included: Hepa1-6, Hep53.4, THP-1, and HEK293T. All cells were cultured in a medium recommended by ATCC, supplemented with 10% fetal bovine serum (FBS; Gibco, USA) and 1% (v/v) streptomycin-penicillin (Sigma-Aldrich, Shanghai, China), and maintained at 37°C in a humidified atmosphere with 5% CO_2. Prior to conducting cell experiments, all the mentioned cell lines underwent testing for short tandem repeat profiling and mycoplasma contamination to ensure their authenticity and purity. Citalopram (S4749), escitalopram (S4064), fluoxetine (S1333), fluvoxamine (S1336), paroxetine (S3005), and sertraline (S4053) were all obtained from Selleck (Shanghai, China).

Plate colony formation assay

For cell proliferation analysis, a total of 1,000 indicated HCC cells were seeded into 6-well plates with three replicates. After treatment with citalopram for 10-14 days, the plates were washed with phosphate-buffered saline (PBS) twice, fixed with methanol for 10 min, and stained with 0.5% (w/v) crystal violet solution for 10 min. Colonies containing more than 30 cells were counted under the microscope.

Detection of Caspase-3/7 activity

Cell apoptosis in HCC cells upon citalopram treatment was assessed using the Apo-ONE® Homogeneous Caspase-3/7 Assay (Promega, Madison, WI, USA) as described previously (Jiang, Li et al., 2017). To normalize the data, the cell viability was detected using CellTiter-Blue (Promega, G8081). The relative Caspase-3/7 activity was determined by calculating the ratio of the signals obtained from the Apo-ONE assay to those from the CellTiter-Blue assay.

Gene knockdown and knockout

The specific shRNA oligonucleotides targeting *Slc6a4* and *Slc2a1* were custom-synthesized by Genepharma (Shanghai, China). Lentivirus packaging was carried out in HEK293T cells using Lipofectamine 2000 (Invitrogen, Carlsbad, CA), and virus titers were determined following standard procedures. HCC cells (Hep53.4 and Hepa1-6) were infected with the virus-containing supernatant in the presence of 6 μg/ml polybrene (Sigma-Aldrich, H9268, St.

Louis, MO) when they reached 70% confluence. Cells expressing the shRNAs were selected using puromycin (2 μg/ml, Gibco, A1113802).

For CRISPR/Cas9-mediated gene knockout, THP-1 cells were initially transfected with the lentiCas9-Blast vector to facilitate the expression of Cas9. To generate *C5AR1*$^{-/-}$ THP-1 cells, a lentiviral system utilizing guide RNA (sgRNA) targeting *C5AR1* was utilized. The lentivirus was produced in HEK293T cells by transfecting lentiGuide-Puro along with packaging plasmids pVSVg and psPAX2. The transfection was carried out using Fugene6 (E2693, Promega) in OptiMEM. After two days, the supernatants were filtered through a 0.45 μm filter, and Cas9-expressing cells were infected with the lentivirus in the presence of 6 μg/ml polybrene. Individual colonies were then seeded into 96-well plates, allowed to reach confluence, and subsequently subjected to knockout efficiency analysis. The sequences for shRNA and sgRNA are provided below: sh*Slc6a4*, CACCGCCTCCTACTATAACACCATCCGAAGATGGTGTTATAGTAGGAGGC; sh*Slc2a1*, CACCGGGAGAAGAAGGTCACCATCTCGAAAGATGGTGACCTTCTTCTCCC; *C5AR1* sgRNA, CTTCAGTCAACACGTTCCGG.

Quantitative real-time PCR (qRT-PCR)

RNA was extracted from CD8^{+} T cells using the RNAiso Plus reagent (Takara, Japan) and subjected to reverse transcription using the PrimeScript RT-PCR kit (Takara, Japan). Then, qRT-PCR was performed using the 7500 Real-time PCR system (Applied Biosystems, USA). The housekeeping gene *Gapdh* was used to normalize gene expression. Primer sequences used in this study were shown below: *Slc2a1* forward, 5'-CAGTTCGGCTATAACACTGGTG-3'; *Slc2a1* reverse, 5'-GCCCCCGACAGAGAAGATG-3'; *Slc2a3* forward, 5'-ATGGGGACAACGAAGGTGAC-3'; *Slc2a3* reverse, 5'-GTCTCAGGTGCATTGATGACTC-3'; *Gapdh* forward, 5'-AGGTCGGTGTGAACGGATTTG-3'; *Gapdh* reverse, 5'-TGTAGACCATGTAGTTGAGGTCA-3'.

Immunoblotting

Cellular lysates were extracted using RIPA lysis buffer (P0013B, Beyotime, Shanghai, China) supplemented with protease and phosphatase inhibitor cocktails (ab201119, Abcam,

Shanghai, China). The protein concentration was quantified with a BCA Protein Assay Kit (Pierce Biotechnology, USA). The proteins were then separated by sodium dodecyl sulfate-polyacrylamide gel electrophoresis (SDS-PAGE) and transferred onto polyvinylidene difluoride (PVDF, Millipore) membranes. Subsequently, the membranes were blocked with 5% (m/v) skim milk for 1 h at room temperature before being incubated with specific antibodies overnight at 4°C. On the following day, the membranes were washed three times with PBS and then incubated with HRP-conjugated secondary antibodies for 45 min. Subsequently, an ECL chemiluminescence assay (SB-WB012, Share-bio, Shanghai, China) was performed using a Bio-Spectrum Gel Imaging System (Bio-Rad). The antibodies utilized in this study included: SERT (1:500, ProteinTech, 19559-1-AP), GLUT1 (1:2,000, Cell Signaling Technology, #73015), GLUT3 (1:1,000, ProteinTech, 20403-1-AP), C5aR1 (1:1,500, ProteinTech, 21316-1-AP), and β-actin (1:2,000, Abcam, ab8226). The information for secondary antibodies is as follows: goat anti-rabbit IgG (H+L) cross-adsorbed secondary antibody (1:5,000, Thermo Fisher Scientific, G-21234) and goat anti-mouse IgG (H+L) cross-adsorbed secondary antibody (1:5,000, Thermo Fisher Scientific, G-21040).

Immunohistochemistry and immunofluorescence analysis

Paraffin-embedded sections of mouse HCC tissues were subjected to immunohistochemical analysis of Ki67, cleaved caspase 3, and C5aR1 expression. Immunohistochemical analysis was performed as reported previously (Jiang et al., 2017). The primary antibodies used in this study were shown as follows: Ki67 (1:400, Cell Signaling Technology, #9449), cleaved caspase 3 (1:400, Cell Signaling Technology, #9661), and C5aR1 (1:1,200, ProteinTech, 21316-1-AP). For immunofluorescence analysis, paraffin sections (5 μm) of HCC samples were deparaffinized and rehydrated with graded ethanol, followed by microwave heating-based antigen retrieval. Then tissue sections were blocked with 10% donkey serum (Sigma-Aldrich, D9663, USA) for 1 h at room temperature and incubated with primary antibodies at 4°C overnight. The following antibodies were used: C5aR1 (1:50, Proteintech, 10375-1-AP) and CD163 (1:200, Abcam, ab182422). The next day, tissue sections were incubated with donkey anti-rabbit Alexa Fluor 594 (1:400, Jackson ImmunoResearch, #711-585-152) and donkey anti-mouse Alexa Fluor 488 (1:400, Jackson ImmunoResearch, #715-545-150) for 30

min at room temperature. Finally, 4',6-diamidino-2-phenylindole (DAPI) staining was performed to visualize the nuclei. Confocal microscope equipped with a digital camera (Nikon, Japan) was used for high-resolution imaging.

Bioinformatics analysis and single cell sequencing data

For GSEA analyses, we conducted RNA sequencing (RNA-seq) analysis on HCC-LM3 cells treated with citalopram or fluvoxamine, which led to the identification of 114 differentially expressed genes (DEGs; 80 co-upregulated and 34 co-downregulated), as reported previously (Dong et al., 2024). These DEGs were then utilized to create an SSRI-related gene signature. Subsequently, we analyzed RNA-seq data from liver HCC (LIHC) samples in The Cancer Genome Atlas (TCGA) cohort, comprising 371 samples, categorizing them into high and low expression groups based on the median expression levels of each candidate target gene. Finally, we performed GSEA on the grouped samples using the SSRI-related gene signature. Correlation analysis was performed with GEPIA2 (http://gepia2.cancer-pku.cn/#index) (Tang, Kang et al., 2019). The following gene signatures were included for analysis, TAMs (*CD33*, *MARCO*, *CXCL5*, *SULT1C2*, *MSR1*, *CTSK*, *PTGDS*, *COLEC12*, *GPC4*, *PCOLCE2*, *CHIT1*, *CLEC5A*, *CCL7*, *FN1*, *CD163*, *GM2A*, *BCAT1*, *RAI14*, *COL8A2*, *CHI3L1*, *ATG7*, *CD84*, *MS4A4A*, *EMP1*, *CYBB*, *CD68*, and *CD11b*), exhausted T cells (*HAVCR2*, *TIGIT*, *LAG3*, *PDCD1*, *CXCL13* and *LAYN*), immune checkpoint (*IDO1*, *IDO2*, *PDCD1*, *CD274*, *PDCD1LG2*, *CTLA4*, *LAG3*, *HAVCR2*, *C10orf54*, *BTLA*, *ICOS*, and *TNFRSF9*), and effector Treg cells (*FOXP3*, *CTLA4*, *CCR8*, and *TNFRSF9*). The single-cell transcriptome expression of C5aR1 and GLUT family members in the tumor microenvironment was identified with GSE125449 and GSE140228-10X.

DARTS experiments

THP-1 or HEK293T cells were lysed using NP40 lysis buffer (Thermo Fisher Scientific, 89842Y). Following centrifugation at 12,000 rpm for 10 min, the supernatant containing the proteins was collected, and the protein concentration was determined using a BCA Protein Assay Kit (Pierce Biotechnology, USA). Samples of equivalent quality were then treated with specific SSRIs and a vehicle at 37°C for 4 h. Subsequently, pronase (10 μg/mL, Roche,

10165921001) or distilled water was added and incubated at room temperature for specified time points (10 and 30 min). The reaction was terminated by adding protease inhibitors, and the resulting products were harvested and subjected to analysis using Western blotting.

In Silico docking study

To predict the binding mode of citalopram/C5aR1, molecular docking was performed using the AutoDock 4.2.6 software package (Morris, Huey et al., 2009). The receptor structure for C5aR1 (PDB id: 6C1Q) (Liu et al., 2018) was sourced from the RCSB protein data bank (https://www.rcsb.org/). Due to the lack of available structural information, the structure of mouse C5aR1 was predicted using a local version of the ColabFold (AlphaFold2) software (Jumper, Evans et al., 2021, Mirdita, Schutze et al., 2022). The original substrates and other heteroatoms in these crystal structures were removed for further docking procedure. The absolute structure of citalopram (CID: 2771), fluoxetine (CID: 3386), fluvoxamine (CID: 5324346), paroxetine (CID: 43815), and sertraline (CID: 68617) were sourced from the PubChem database (https://pubchem.ncbi.nlm.nih.gov/). In each docking scenario, molecular docking was conducted following a standard protocol (Forli, Huey et al., 2016), with a modification in the number of genetic algorithm runs to 500 to comprehensively explore the binding modes. The binding energy and cluster information were directly extracted from the AutoDock output.

Biochemical analysis

The serum levels of inflammatory cytokines (TNF-α, IL-1β, and IL-6) were analyzed using commercial ELISA kits following the manufacturer's instructions (R&D Systems). The cytokine concentrations were calculated using a standard curve, and the data were presented in picograms per milliliter. Serum 5-HT levels were assessed using the 5-HT ELISA Kit from Abcam (ab133053), following the manufacturer's guidelines.

Isolation of TAMs from xenograft tumor tissues

Fresh sterile tumor tissues from subcutaneous xenograft model were washed with PBS two times, minced with scalpels, and then digested using a Tumor Dissociation Kit (Miltenyi Biotec,

cat #130-095-929) at room temperature for 30 min. Digested tumor tissues were filtered through Falcon 70Micrometer Cell Strainer (Corning, #352350) and centrifuged at 1,500 rpm for 5 min. Red blood cells were removed using Red Blood Cell Lysis Solution (Miltenyi Biotec, cat #130-094-183). Then, TAMs were selected by CD11b microbeads (Miltenyi Biotec, cat #130-049- 601) according to the manufacturer's instructions.

Isolation of immune cells and flow cytometry

Mice were euthanized, and fresh tumor tissues and spleen were harvested. Spleens were mechanically disrupted through 70 μm Nylon mesh (Corning, #352350) to release single cells. The cells were washed with PBS, followed by the lysis of red blood cells with Red Blood Cell Lysis Solution (Miltenyi Biotec, cat #130-094-183). Tumor tissues were cut into small pieces with surgical scissors and digested with 2 mg/mL collagenase IV (Sigma) for 20 min and filtered with 70 μm Nylon mesh. The isolated cells were collected with PBS and subjected to centrifuged at 1,500 rpm for 5 min. To enrich immunocytes from tumor tissues, harvested cells were centrifuged through different concentrations of discontinuous gradients of 40/80 Percoll (GE Healthcare, cat #17-0891-01) at 350 × g for 30 min. The middle pellet was washed with PBS, subjected to red blood cell lysis for 3 min.

For staining molecules expressed on cell surface, single cell suspensions from spleens and tumor tissues were labeled with fluorophore-conjugated antibodies: PerCP-Cyanine 5.5 7AAD (Biolegend, Cat #420404, 1:1,000), FITC anti-mouse CD4 (Biolegend, Cat #100406, 1:1,000), PE anti-mouse Ly6G (Biolegend, Cat #127608, 1:200), APC anti-mouse CD11c antibody (Biolegend, Cat #117310, 1:200), PE-cy7 anti-mouse CD8α (Biolegend, Cat #100722, 1:200), Brilliant Violet 421 anti-mouse CD3 (Biolegend, Cat #100227, 1:200), Alex Fluor 647 anti-mouse F4/80 (Invitrogen, Cat #2604384, 1:200), Brilliant Violet 510 anti-mouse CD45 (Biolegend, Cat #103138, 1:200), PE-cy7 anti-mouse NK1.1 (Biolegend, Cat #156513, 1:200), Brilliant Violet 421 anti-mouse B220 (Biolegend, Cat #103240, 1:200), Brilliant Violet 605 anti-mouse CD11b (Biolegend, Cat #101257, 1:200), APC-CY7 Stain 780 (BD Bioscience, Cat #565388, 1:1,000).

For intracellular staining, single cell suspensions from tumor tissues were stimulated with Cell Stimulation Cocktail (Invitrogen) for 4 h, and labeled with PE anti-mouse CD45 antibody

(Biolegend, Cat #103106, 1:200), PerCP-Cyanine 5.5 CD3 (Biolegend, Cat #100325, 1:200), PE-cy7 anti-mouse CD8a (Biolegend, Cat# 100722, 1:200), APC-CY7 Stain 780 (BD Bioscience, Cat #565388, 1:1,000). After fixation and permeabilization using the Fix/Perm kit (ThermoFisher, GAS004), cells were labeled with APC anti-human/mouse Granzyme B Recombinant antibody (Biolegend, Catalog no.372203, 1:200), Brilliant Violet 421 anti-mouse IFN-γ (Biolegend, Cat #505830, 1:200), Brilliant Violet 605 anti-mouse TNF-α (Biolegend, Cat #506329, 1:200). Flow cytometry was performed in BD FACSCanto II.

T cell activation, expansion and cytotoxicity

Single-cell suspensions were freshly dissected from the spleen and lymph nodes, and red blood cells were removed using Red Blood Cell Lysis Solution (Miltenyi Biotec, cat #130-094-183). $CD8^+$ T cells were isolated from the resulting cell suspensions by $CD8^+$ magnetic bead selection (Miltenyi Biotec, cat #130-117-044). For T cell proliferation assay, isolated $CD8^+$ T cells were resuspended in PBS supplemented with carboxy fluorescein succinimidyl ester (CFSE, Invitrogen, 1:10,000) for 8 min at room temperature and washed with RPMI 1640, supplemented with 10% heat-inactivated FBS. Then, $CD8^+$ T cells were activated by plate-bound αCD3ε (5 μg/mL, Biolegend, Catalog no.100359) and α-CD28 (2 μg/mL, Biolegend, Catalog no.102121) in complete RPMI 1640 medium at 37°C and 5% CO_2 for 72 h in the presence or absence of 5 μM citalopram treatment. Finally, cell proliferation was assessed by flow cytometry. For assessment of cellular activation and cytotoxicity, $CD8^+$ T cells were stimulated by Leukocyte Activation Cocktail (GolgiPlug™ BD, Catalog no.550583) for 4 h, resuspended in PBS/2% FBS containing PE anti-mouse CD62L antibody (Biolegend, Catalog no.104407, 1:200) and Brilliant Violet 510 anti-mouse/human CD44 Antibody (Biolegend, Catalog no.103044, 1:200), followed by incubation at room temperature for 30 min and washed in PBS/2% FBS. After fixation and permeabilization using the Cytofix/Cytoperm solution (BD Biosciences) for 20 min at 4°C, Brilliant Violet 421 anti-mouse IFN-γ antibody (Biolegend, Catalog no.505830, 1:200), APC anti-human/mouse Granzyme B Recombinant antibody (Biolegend, Catalog no.372203, 1:200) and Alexa Fluor 488 anti-mouse TNF-α antibody (Biolegend, Catalog no. 506313, 1:200) were employed for intracellular staining. Then, cell activation and cytotoxicity were assessed by flow cytometry.

Macrophage phagocytosis assay

Phagocytosis assays of tumor cells were performed as previously described (Chen, Zhong et al., 2017). Briefly, 5 × 10^4 phorbol myristate acetate (PMA, 100 ng/ml) primed THP-1 cells and harvested TAMs were seeded overnight in a 24-well tissue culture plate. The next day, HCC-LM3 cells and Hepa1-6 cells were labelled with pHrodo™ Green (Thermo, Cat #P35373, 1:1,000). After incubating macrophages in serum-free medium for 2 h, the macrophages were labeled with CellTracker™ Deep Red Dye (Thermo, Cat #C34565, 6 ng/mL). Then, 5 × 10^4 predyed tumor cells were added to the macrophages, in the presence or absence of C5a stimulation and different SSRIs (5 μM). After incubation at 37 °C for 4 h, macrophages were extensively washed and imaged with Confocal Laser Scanning Microscope (Leica).

Macrophage depletion assay

The method for eliminating macrophages was reported previously (Jiang, Zhu et al., 2019). Briefly, C57BL/6 mice were intraperitoneally injected with clodronate liposomes (1.4 mg/20 g body weight) to remove macrophages. Clodronate liposomes (Yeasen, 40337ES10, Shanghai, China) were given every three days for 12 days before tumor inoculation. After inoculation of sh*Slc2a1* ($GLUT1^{KD}$) Hepa1-6 cells, clodronate liposomes were also administered every three days until the end of the experiment. When the mice were sacrificed, liver and tumor tissues were extracted, and F4/80 staining (1:250, Cell Signaling Technology, #70076) was performed to determine the efficiency of macrophage depletion.

$CD4^+$ T cell and $CD8^+$ T cell depletion experiments

For $CD4^+$ T and $CD8^+$ T cell depletion, mice were treated intraperitoneally with 200 μg of specific monoclonal antibodies (Ultra-LEAF™ Purified anti-mouse CD8a Antibody, Biolegend, cat #100763; and Ultra-LEAF™ Purified anti-mouse CD4 Antibody, Biolegend, cat #100457) the day before the implantation of cancer cells and then with 100 μg twice a week for the entire duration of the experiment.

Statistical analysis.

The sample sizes for *in vitro* and *in vivo* studies determined based on similar studies in the field and through pilot studies. Details regarding sample sizes and biological replicates can be found in the figure legends. Continuous variables are presented as means ± SD. For comparisons between two independent groups, a two-tailed Student's t-test was employed. Statistical analyses involving more than two groups were conducted using either a one-way analysis of variance (ANOVA) with Tukey's method or two-way ANOVA with Dunnett multiple comparisons, as specified. GraphPad Prism 9 (GraphPad Software Inc., San Diego, CA) was used for statistical analyses. Kaplan-Meier survival curves were generated and analyzed using the log-rank test. A p-value less than 0.05 was considered statistically significant. In all figures, statistical significance is represented as follows: *$p < 0.05$; **$p < 0.01$; ***$p < 0.001$.

ACKNOWLEDGMENTS

The research was supported by grants from National Natural Science Foundation of China (82472883), Shanghai Pilot Program for Basic Research-Shanghai Jiao Tong University (21TQ1400225), China Foundation For Youth Entrepreneurship and Employment (P24062487785), "Rising Stars of Medical Talents" Youth Development Program (Youth Medical Talents-Specialist Program), Clinical Medicine Research Center Construction Project of Huadong Hospital (LCZX2202), Shanghai Outstanding Young Medical Personnel Training Program & Excellence Project of Shanghai Municipal Health Commission (20224Z0009), Key specialized diseases construction of Huadong Hospital (ZDZB2225), and Key Areas Research and Development Programs of Guangdong Province (2023B1111050009).

AUTHOR CONTRIBUTIONS

Conceptualization: S.H.J.; Methodology: F.D., S.H.J., K.S., S.Z., and L.J.J.; Formal Analysis: F.D., S.H.J., S.Z. and L.J.J.; Resources: M.X.F., X. W. and S.H.J.; Investigation: all authors; Supervision: S.H.J., X. W. and Z.G.Z.; Funding Acquisition: S.H.J., Z.G.Z., Z.B. and F.D.; Writing-Original Draft: F.D., K.S., S.Z., L.J.J. and S.H.J; Writing-Review & Editing: all authors.

DECLARATION OF INTERESTS

The authors declare no conflicts of interest.

References

Ajona D, Zandueta C, Corrales L, Moreno H, Pajares MJ, Ortiz-Espinosa S, Martínez-Terroba E, Perurena N, de Miguel FJ, Jantus-Lewintre E, Camps C, Vicent S, Agorreta J, Montuenga LM, Pio R, Lecanda F (2018) Blockade of the Complement C5a/C5aR1 Axis Impairs Lung Cancer Bone Metastasis by CXCL16-mediated Effects. *Am J Resp Crit Care* 197: 1164-1176

Beach C, MacLean D, Majorova D, Melemenidis S, Nambiar DK, Kim RK, Valbuena GN, Guglietta S, Krieg C, Darvish-Damavandi M, Suwa T, Easton A, Hillson LVS, McCulloch AK, McMahon RK, Pennel K, Edwards J, O'Cathail SM, Roxburgh CS, Domingo E et al. (2023) Improving radiotherapy in immunosuppressive microenvironments by targeting complement receptor C5aR1. *Journal of Clinical Investigation* 133: e168277

Bhagavathula AS, Woolf B, Rahmani J, Vidyasagar K, Tesfaye W (2022) Selective serotonin reuptake inhibitor use and the risk of hepatocellular carcinoma: a systematic review and dose-response analysis of cohort studies with one million participants. *Eur J Clin Pharmacol* 78: 547-555

Bi JF, Khan A, Tang J, Armando AM, Wu SH, Zhang W, Gimple RC, Reed A, Jing H, Koga T, Wong ITL, Gu YC, Miki S, Yang HJ, Prager B, Curtis EJ, Wainwright DA, Furnari FB, Rich JN, Cloughesy TF et al. (2021) Targeting glioblastoma signaling and metabolism with a re-purposed brain-penetrant drug. *Cell reports* 37: 109957

Cao J, Liao S, Zeng F, Liao Q, Luo G, Zhou Y (2023) Effects of altered glycolysis levels on CD8+ T cell activation and function. *Cell death & disease* 14: 407

Carlson LE, Ismaila N, Addington EL, Asher GN, Atreya C, Balneaves LG, Bradt J, Fuller-Shavel N, Goodman J, Hoffman CJ, Huston A, Mehta A, Paller CJ, Richardson K, Seely D, Siwik CJ, Temel JS, Rowland JH (2023) Integrative Oncology Care of Symptoms of Anxiety and Depression in Adults With Cancer: Society for Integrative Oncology-ASCO Guideline. *J Clin Oncol* 41: 4562-4591

Chen J, Zhong MC, Guo HJ, Davidson D, Mishel S, Lu Y, Rhee I, Perez-Quintero LA, Zhang SH, Cruz-Munoz ME, Wu N, Vinh DC, Sinha M, Calderon V, Lowell CA, Danska JS, Veillette A (2017) SLAMF7 is critical for phagocytosis of haematopoietic tumour cells via Mac-1 integrin. *Nature* 544: 493-497

Coleman JA, Green EM, Gouaux E (2016) X-ray structures and mechanism of the human serotonin transporter. *Nature* 532: 334-9

Costa LHA, Santos BM, Branco LGS (2020) Can selective serotonin reuptake inhibitors have a neuroprotective effect during COVID-19? *Eur J Pharmacol* 889: 173629

Custódio TF, Paulsen PA, Frain KM, Pedersen BP (2021) Structural comparison of GLUT1 to GLUT3 reveal transport regulation mechanism in sugar porter family. *Life Sci Alliance* 4: e202000858

Ding P, Li L, Li L, Lv X, Zhou D, Wang Q, Chen J, Yang C, Xu E, Dai W, Zhang X, Wang N,

Wang Q, Zhang W, Zhang L, Zhou Y, Gu H, Lei Q, Zhou X, Hu W (2020) C5aR1 is a master regulator in Colorectal Tumorigenesis via Immune modulation. *Theranostics* 10: 8619-8632

Dong FY, He K, Zhang S, Song KY, Jiang LJ, Hu LP, Li Q, Zhang XL, Zhang NQ, Li BT, Zhu LL, Li J, Feng MX, Gao YC, Chen J, Hu XA, Wang JF, Jiang CY, Wang C, Zhu HH et al. (2024) SSRI antidepressant citalopram reverses the Warburg effect to inhibit hepatocellular carcinoma by directly targeting GLUT1. *Cell reports* 43: 114818

Du DY, Liu C, Qin MY, Zhang X, Xi T, Yuan ST, Hao HP, Xiong J (2022) Metabolic dysregulation and emerging therapeutical targets for hepatocellular carcinoma. *Acta Pharm Sin B* 12: 558-580

Eslam M, Newsome PN, Sarin SK, Anstee QM, Targher G, Romero-Gomez M, Zelber-Sagi S, Wong VWS, Dufour JF, Schattenberg JM, Kawaguchi T, Arrese M, Valenti L, Shiha G, Tiribelli C, Yki-Järvinen H, Fan JG, Gronbæk H, Yilmaz Y, Cortez-Pinto H et al. (2020) A new definition for metabolic dysfunction-associated fatty liver disease: An international expert consensus statement. *Journal of hepatology* 73: 202-209

Fischer A, Rennert HS, Rennert G (2022) Selective serotonin reuptake inhibitors associated with increased mortality risk in breast cancer patients in Northern Israel. *International journal of epidemiology* 51: 807-816

Fluyau D, Mitra P, Jain A, Kailasam VK, Pierre CG (2022) Selective serotonin reuptake inhibitors in the treatment of depression, anxiety, and post-traumatic stress disorder in substance use disorders: a Bayesian meta-analysis. *Eur J Clin Pharmacol* 78: 931-942

Foretz M, Guigas B, Viollet B (2023) Metformin: update on mechanisms of action and repurposing potential. *Nat Rev Endocrinol* 19: 460-476

Forli S, Huey R, Pique ME, Sanner MF, Goodsell DS, Olson AJ (2016) Computational protein-ligand docking and virtual drug screening with the AutoDock suite. *Nature protocols* 11: 905-19

Hochrein SM, Wu H, Eckstein M, Arrigoni L, Herman JS, Schumacher F, Gerecke C, Rosenfeldt M, Gru D, Kleuser B, Gasteiger G, Kastenmu W, Ghesquiere B, Van den Bossche J, Abel ED, Vaeth M (2022) The glucose transporter GLUT3 controls T helper 17 cell responses through glycolytic-epigenetic reprogramming. *Cell metabolism* 34: 516-532

Huang KL, Chen YL, Stewart R, Chen VCH (2023) Antidepressant Use and Mortality Among Patients With Hepatocellular Carcinoma. *Jama Netw Open* 6: e2332579

Hwang HY, Shim JS, Kim D, Kwon HJ (2021) Antidepressant drug sertraline modulates AMPK-MTOR signaling-mediated autophagy via targeting mitochondrial VDAC1 protein. *Autophagy* 17: 2783-2799

Jiang SH, Li J, Dong FY, Yang JY, Liu DJ, Yang XM, Wang YH, Yang MW, Fu XL, Zhang XX, Li Q, Pang XF, Huo YM, Li J, Zhang JF, Lee HY, Lee SJ, Qin WX, Gu JR, Sun YW et al. (2017) Increased Serotonin Signaling Contributes to the Warburg Effect in Pancreatic Tumor Cells Under Metabolic Stress and Promotes Growth of Pancreatic Tumors in Mice. *Gastroenterology* 153: 277-291 e19

Jiang SH, Wang YH, Hu LP, Wang X, Li J, Zhang XL, Zhang ZG (2021) The physiology,

pathology and potential therapeutic application of serotonylation. *Journal of cell science* 134: jcs257337

Jiang SH, Zhu LL, Zhang M, Li RK, Yang Q, Yan JY, Zhang C, Yang JY, Dong FY, Dai M, Hu LP, Li J, Li Q, Wang YH, Yang XM, Zhang YL, Nie HZ, Zhu L, Zhang XL, Tian GA et al. (2019) GABRP regulates chemokine signalling, macrophage recruitment and tumour progression in pancreatic cancer through tuning KCNN4-mediated Ca(2+) signalling in a GABA-independent manner. *Gut* 68: 1994-2006

Jumper J, Evans R, Pritzel A, Green T, Figurnov M, Ronneberger O, Tunyasuvunakool K, Bates R, Zidek A, Potapenko A, Bridgland A, Meyer C, Kohl SAA, Ballard AJ, Cowie A, Romera-Paredes B, Nikolov S, Jain R, Adler J, Back T et al. (2021) Highly accurate protein structure prediction with AlphaFold. *Nature* 596: 583-589

Lee MJ, Huang CW, Chen YL, Yang YH, Chen VCH (2021) Association between selective serotonin reuptake inhibitors and kidney cancer risk: A nationwide population-based cohort study. *International journal of cancer* 148: 1331-1337

Li B, Elsten-Brown J, Li M, Zhu EB, Li Z, Chen YN, Kang EL, Ma FY, Chiang JNF, Li YR, Zhu YC, Huang J, Fung A, Scarborough Q, Cadd R, Zhou JJ, Chin AI, Pellegrini M, Yang LL (2025) Serotonin transporter inhibits antitumor immunity through regulating the intratumoral serotonin axis. *Cell* 188: 3823-3842

Li X, Poire A, Jeong KJ, Zhang D, Ozmen TY, Chen G, Sun CY, Mills GB (2024) C5aR1 inhibition reprograms tumor associated macrophages and reverses PARP inhibitor resistance in breast cancer. *Nature communications* 15: 4485

Liu H, Kim HR, Deepak R, Wang L, Chung KY, Fan H, Wei Z, Zhang C (2018) Orthosteric and allosteric action of the C5a receptor antagonists. *Nat Struct Mol Biol* 25: 472-481

Llovet JM, Castet F, Heikenwalder M, Maini MK, Mazzaferro V, Pinato DJ, Pikarsky E, Zhu AX, Finn RS (2022) Immunotherapies for hepatocellular carcinoma. *Nature reviews Clinical oncology* 19: 151-172

Lomenick B, Hao R, Jonai N, Chin RM, Aghajan M, Warburton S, Wang JN, Wu RP, Gomez F, Loo JA, Wohlschlegel JA, Vondriska TM, Pelletier J, Herschman HR, Clardy J, Clarke CF, Huang J (2009) Target identification using drug affinity responsive target stability (DARTS). *Proceedings of the National Academy of Sciences of the United States of America* 106: 21984-21989

Luan XJ, Lei T, Fang J, Liu X, Fu HJ, Li YR, Chu W, Jiang P, Tong C, Qi HB, Fu Y (2024) Blockade of C5a receptor unleashes tumor-associated macrophage antitumor response and enhances CXCL9-dependent CD8+T cell activity. *Molecular Therapy* 32: 469-489

Macintyre AN, Gerriets VA, Nichols AG, Michalek RD, Rudolph MC, Deoliveira D, Anderson SM, Abel ED, Chen BJ, Hale LP, Rathmell JC (2014) The Glucose Transporter Glut1 Is Selectively Essential for CD4 T Cell Activation and Effector Function. *Cell metabolism* 20: 61-72

Medler TR, Murugan D, Horton W, Kumar S, Cotechini T, Forsyth AM, Leyshock P, Leitenberger JJ, Kulesz-Martin M, Margolin AA, Werb Z, Coussens LM (2018) Complement

C5a Fosters Squamous Carcinogenesis and Limits T Cell Response to Chemotherapy. *Cancer cell* 34: 561- 578 e6

Mirdita M, Schutze K, Moriwaki Y, Heo L, Ovchinnikov S, Steinegger M (2022) ColabFold: making protein folding accessible to all. *Nat Methods* 19: 679-682

Morris GM, Huey R, Lindstrom W, Sanner MF, Belew RK, Goodsell DS, Olson AJ (2009) AutoDock4 and AutoDockTools4: Automated docking with selective receptor flexibility. *Journal of computational chemistry* 30: 2785-91

Ou B, Liu Y, Yang X, Xu X, Yan Y, Zhang J (2021) C5aR1-positive neutrophils promote breast cancer glycolysis through WTAP-dependent m6A methylation of ENO1. *Cell death & disease* 12: 737

Pio R, Ajona D, Ortiz-Espinosa S, Mantovani A, Lambris JD (2019) Complementing the Cancer-Immunity Cycle. *Front Immunol* 10: 774

Pushpakom S, Iorio F, Eyers PA, Escott KJ, Hopper S, Wells A, Doig A, Guilliams T, Latimer J, McNamee C, Norris A, Sanseau P, Cavalla D, Pirmohamed M (2019) Drug repurposing: progress, challenges and recommendations. *Nature Reviews Drug Discovery* 18: 41-58

Robertson N, Rappas M, Dore AS, Brown J, Bottegoni G, Koglin M, Cansfield J, Jazayeri A, Cooke RM, Marshall FH (2018) Structure of the complement C5a receptor bound to the extra-helical antagonist NDT9513727. *Nature* 553: 111-114

Schipper LJ, Zeverijn LJ, Garnett MJ, Voest EE (2022) Can Drug Repurposing Accelerate Precision Oncology? *Cancer discovery* 12: 1634-1641

Schneider MA, Heeb L, Beffinger MM, Pantelyushin S, Linecker M, Roth L, Lehmann K, Ungethum U, Kobold S, Graf R, Van den Broek M, Vom Berg J, Gupta A, Clavien PA (2021) Attenuation of peripheral serotonin inhibits tumor growth and enhances immune checkpoint blockade therapy in murine tumor models. *Science Translational Medicine* 13: eabc8188

Singh I, Seth A, Billesbolle CB, Braz J, Rodriguiz RM, Roy K, Bekele B, Craik V, Huang XP, Boytsov D, Pogorelov VM, Lak P, O'Donnell H, Sandtner W, Irwin JJ, Roth BL, Basbaum AI, Wetsel WC, Manglik A, Shoichet BK et al. (2023) Structure-based discovery of conformationally selective inhibitors of the serotonin transporter. *Cell* 186: 2160-2175 e17

Tang Z, Kang B, Li C, Chen T, Zhang Z (2019) GEPIA2: an enhanced web server for large-scale expression profiling and interactive analysis. *Nucleic acids research* 47: W556-W560

Wang LP, Liang DL, Huang YY, Chen YX, Yang XC, Huang ZJ, Jiang YQ, Su HF, Wang LJ, Pathak JL, Ge LH (2023) SAP deficiency aggravates periodontitis possibly via C5a-C5aR signaling-mediated defective macrophage phagocytosis of Porphyromonas gingivalis. *J Adv Res* 50: 55-68

Wang X, Fu SQ, Yuan X, Yu F, Ji Q, Tang HW, Li RK, Huang S, Huang PQ, Qin WT, Zuo H, Du C, Yao LL, Li H, Li J, Li DX, Yang Y, Xiao SY, Tulamaiti A, Wang XF et al. (2024) A GAPDH serotonylation system couples CD8+T cell glycolytic metabolism to antitumor immunity. *Molecular cell* 84: 760-775 e7

Wang Y, Liu W, Xu Y, He X, Yuan Q, Luo P, Fan W, Zhu J, Zhang X, Cheng X, Jiang Y, Xu HE, Zhuang Y (2023) Revealing the signaling of complement receptors C3aR and C5aR1 by

anaphylatoxins. *Nat Chem Biol* 19: 1351-1360

Xia Y, Sun M, Huang H, Jin WL (2024) Drug repurposing for cancer therapy. *Signal Transduct Target Ther* 9: 92

Zhang NQ, Sundquist J, Sundquist K, Zhang ZG, Ji JG (2021) Combined Use of Aspirin and Selective Serotonin Reuptake Inhibitors Is Associated With Lower Risk of Colorectal Cancer: A Nested Case-Control Study. *Am J Gastroenterol* 116: 1313-1321

Zhang QM, He Y, Luo N, Patel SJ, Han YJ, Gao RR, Modak M, Carotta S, Haslinger C, Kind D, Peet GW, Zhong GJ, Lu SJ, Zhu WH, Mao YL, Xiao MM, Bergmann M, Hu XD, Kerkar SP, Vogt AB et al. (2019) Landscape and Dynamics of Single Immune Cells in Hepatocellular Carcinoma. *Cell* 179: 829-845 e20

Zhao J, Yao C, Qin YQ, Zhu HY, Guo H, Ji BB, Li XQ, Sun N, Li RQ, Wu YZ, Zheng KY, Pan YC, Zhao TT, Yang J (2024) Blockade of C5aR1 resets M1 via gut microbiota-mediated PFKM stabilization in a TLR5-dependent manner. *Cell death & disease* 15: 120

Zheng Y, Wang S, Cai J, Ke A, Fan J (2021) The progress of immune checkpoint therapy in primary liver cancer. *Biochimica et biophysica acta Reviews on cancer* 1876: 188638

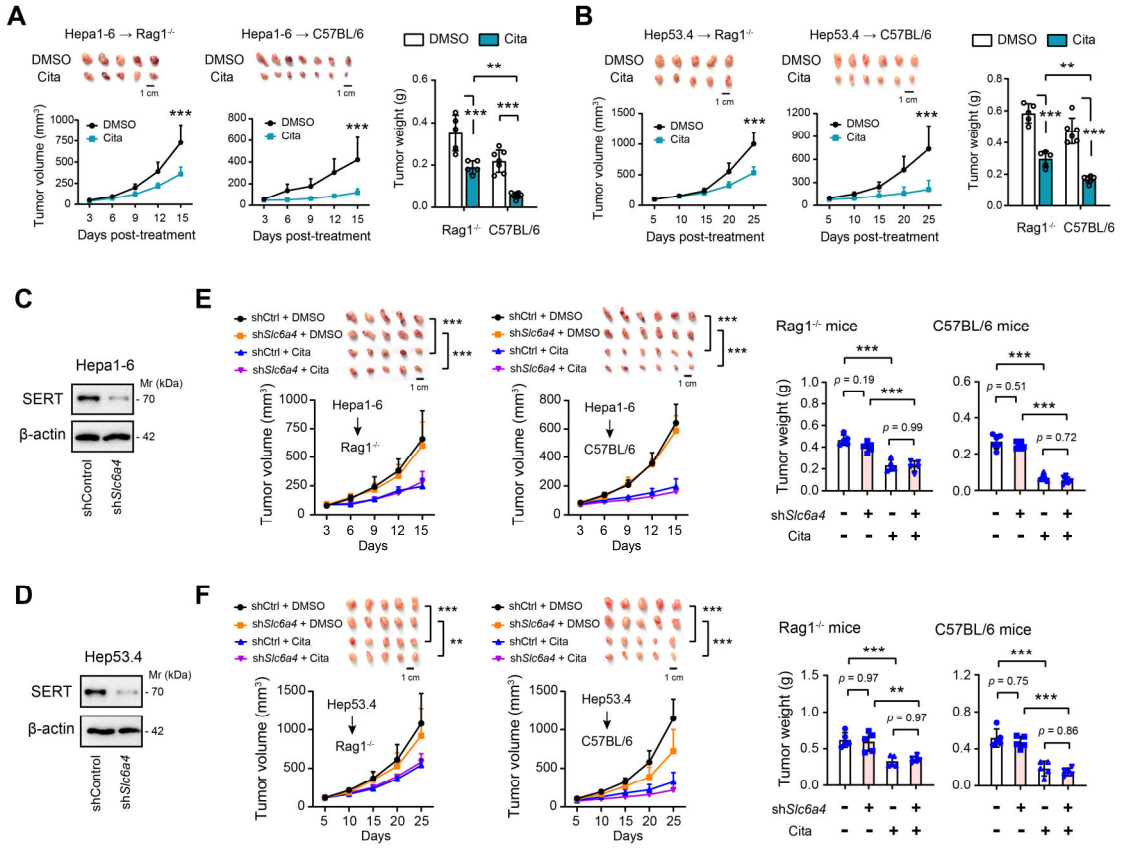

Figure 1. The immune-dependent and SERT-independent anti-tumor effects of citalopram in HCC.

(**A**, **B**) Mouse HCC cells, Hepa1-6 or Hep53.4, were subcutaneously injected into *Rag1*$^{-/-}$ C57BL/6 or immunocompetent C57BL/6 mice (n = 5-7 per group). When bore visible tumors, 5 mg/kg citalopram was treated daily for 15 or 25 days. Tumors were excised after mice were sacrificed, and the tumor weight was measured. (**C**, **D**) Western blotting showed the knockdown efficiency of SERT in Hepa1-6 and Hep53.4 cells. (**E**, **F**) shControl and sh*Slc6a4* Hepa1-6 and Hep53.4 cells were subcutaneously injected into *Rag1*$^{-/-}$ C57BL/6 or immunocompetent C57BL/6 mice (n = 5-6 per group). When bore visible tumors, 5 mg/kg citalopram was treated daily for 15 or 25 days. Tumors were excised after mice were sacrificed, and the tumor weight was measured. In all panels, *$p < 0.05$, **$p < 0.01$, ***$p < 0.001$. Values as mean ± SD and compared by one-way ANOVA multiple comparisons with Tukey's method (for bar chart comparison) and two-way ANOVA with Dunnett's multiple comparisons (for survival curve comparison).

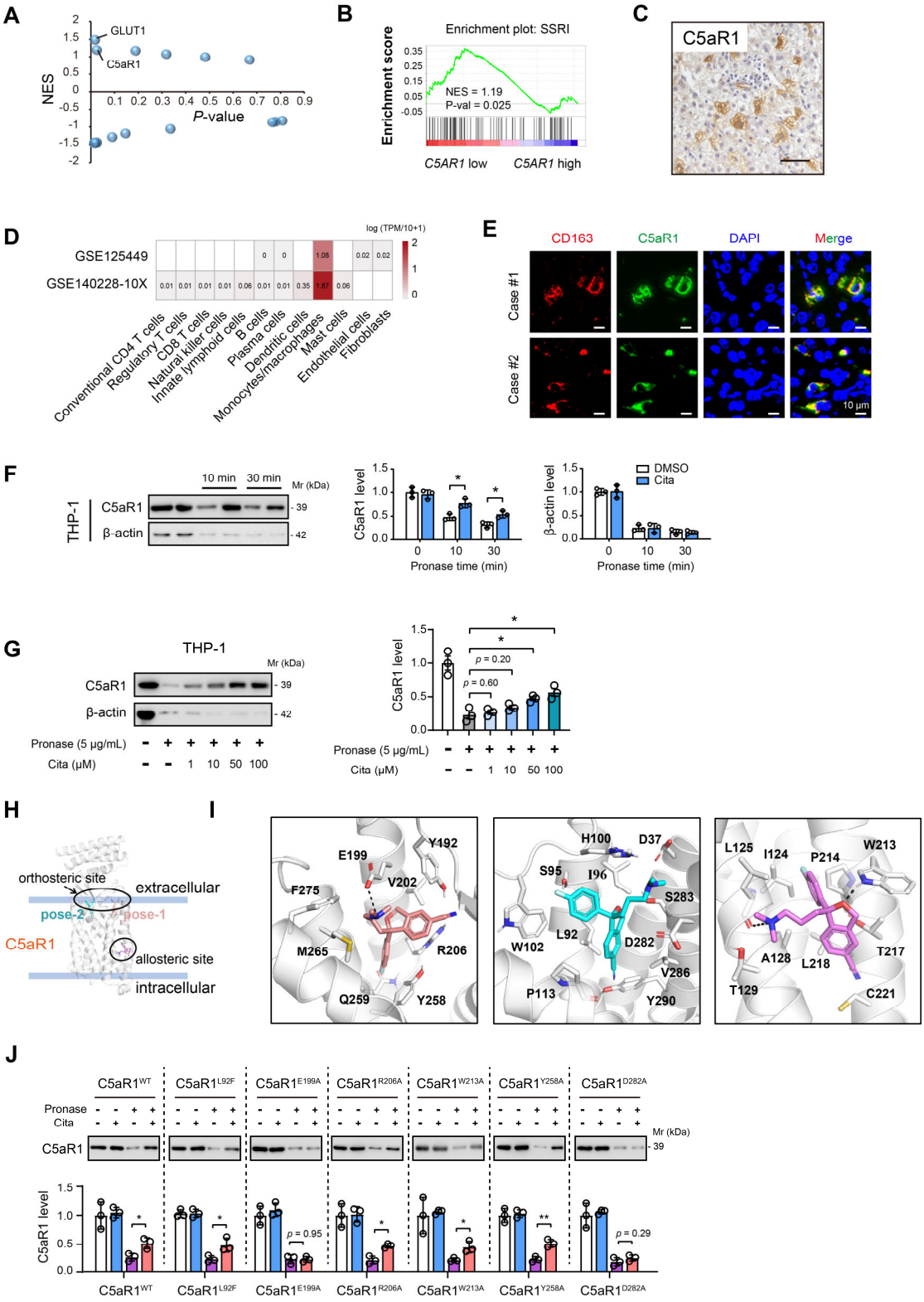

Figure 2. C5aR1 is a direct target of citalopram.

(**A**) Gene Set Enrichment Analysis (GSEA) identified GLUT1 and C5aR1 as two top hits related to SSRI-induced gene changes. (**B**) GSEA of HCC RNAseq data (TCGA cohort) with the SSRI-related gene signature. Sample grouping was made based on the median

expression of C5aR1. (**C**) Representative immunohistochemical images showed the expression pattern and cellular distribution of C5aR1 in human HCC tissues. Scale bar, 50 μm. (**D**) Single cell RNA sequencing analysis showed the expression pattern of C5aR1 with the immune microenvironment of HCC. (**E**) Co-immunofluorescence of C5aR1 (green) with CD163 (red) in HCC samples. Scale bar, 10 μm. (**F**) The DARTS assay and immunoblot analysis showed C5aR1 protein stability against 5 μg/mL pronase in the presence and absence of 100 μM citalopram treatment. (**G**) The DARTS assay and immunoblot analysis showed C5aR1 protein stability against 5 μg/mL pronase in the presence of different concentration of citalopram treatment. (**H**) The overall conformation of citalopram binding to C5aR1. (**I**) Representative models of citalopram in pose-1 (left), pose-2 (middle) and allosteric site (right). Several polar interactions were indicated by black dashed lines. (**J**) HEK293T cells were transfected with either WT or mutant C5aR1 expression plasmids for 48 h, followed by DARTS assay with immunoblotting analysis of C5aR1 protein levels. In all panels, $^{*}p < 0.05$, $^{**}p < 0.01$. Values as mean ± SD and compared by the Student's t test (**F**) or one-way ANOVA multiple comparisons with Tukey's method among groups (**G**, **J**).

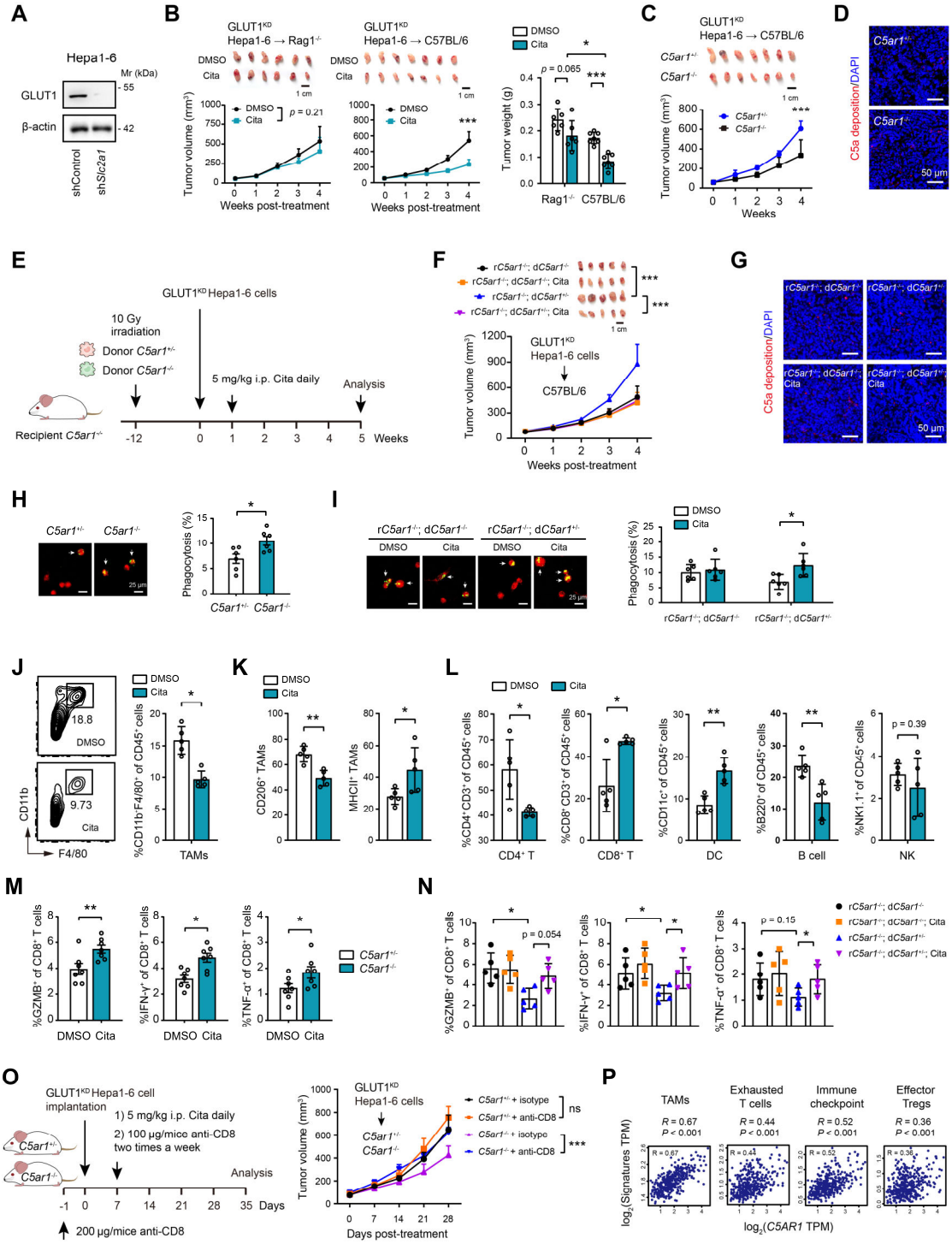

Figure 3. Citalopram targets C5aR1⁺ TAMs

(**A**) Western blotting showed the knockdown efficiency of GLUT1 in mouse Hepa1-6 cells. (**B**) GLUT1^{KD} Hepa1-6 cells were subcutaneously injected into the *Rag1*$^{-/-}$ or immunocompetent C57BL/6 mice, and mice were treated with 5 mg/kg citalopram when bore visible tumors; three weeks later, tumor burden was examined (n = 6-7 per group). (**C**) The growth kinetics of GLUT1^{KD} Hepa1-6 tumors in *C5ar1*$^{+/-}$ and *C5ar1*$^{-/-}$ C57BL/6 host (n = 7). (**D**)

Immunofluorescence analysis of C5a deposition in GLUT1^{KD} Hepa1-6 tumors from *C5ar1*$^{+/-}$ and *C5ar1*$^{-/-}$ C57BL/6 host. Scale bar, 50 μm. (**E**) Experimental design of bone marrow transfer experiments. (**F**, **G**, **I**) GLUT1^{KD} Hepa1-6 cells were subcutaneously implanted into syngeneic recipient (r) mice that had been reconstituted with bone marrow cells from either *C5ar1*$^{+/-}$ or *C5ar1*$^{-/-}$ donor mice. The therapeutic effect of citalopram (**F**), C5a deposition (**G**), and macrophage phagocytosis (**I**) in this model were analyzed. Scale bar, 50 μm. (**H**) The phagocytic capacity of macrophages isolated from GLUT1^{KD} Hepa1-6 tumors in *C5ar1*$^{+/-}$ and *C5ar1*$^{-/-}$ C57BL/6 host. (**J-L**) Flow cytometry showed the infiltration of CD45^{+}CD11b^{+}F4/80^{+} macrophages (**J**), CD206^{+} TAMs and CD11b^{+} TAMs (**K**), tumor-infiltrating lymphocytes (**L**) in tumor tissues from orthotopic xenograft model, which generated in immunocompetent C57BL/6 mice with Hepa1-6 cells (n = 5 per group). (**M, N**) Measurement of CD8^{+} T cell function in tumor tissues from the groups mentioned in **C** and **F**. (**O**) The growth kinetics of GLUT1^{KD} Hepa1-6 tumors in *C5ar1*$^{+/-}$ and *C5ar1*$^{-/-}$ C57BL/6 host upon CD8^{+} T cell depletion (n = 7). (**P**) Correlation analysis of C5aR1 expression and immune checkpoint molecules, gene signatures of TAMs, exhausted T cells, and effector Tregs in the TCGA cohort (n = 371). In all panels, *$p < 0.05$, **$p < 0.01$, ***$p < 0.001$; ns, non-significant. Values as mean ± SD and compared by two-way ANOVA with Dunnett's multiple comparisons (**B**, **C**, **F**, **O**), Student's t test (**H**-**M**), one-way ANOVA multiple comparisons with Tukey's method (**B**, **N**), and the Spearman's rank correlation methods (**P**).

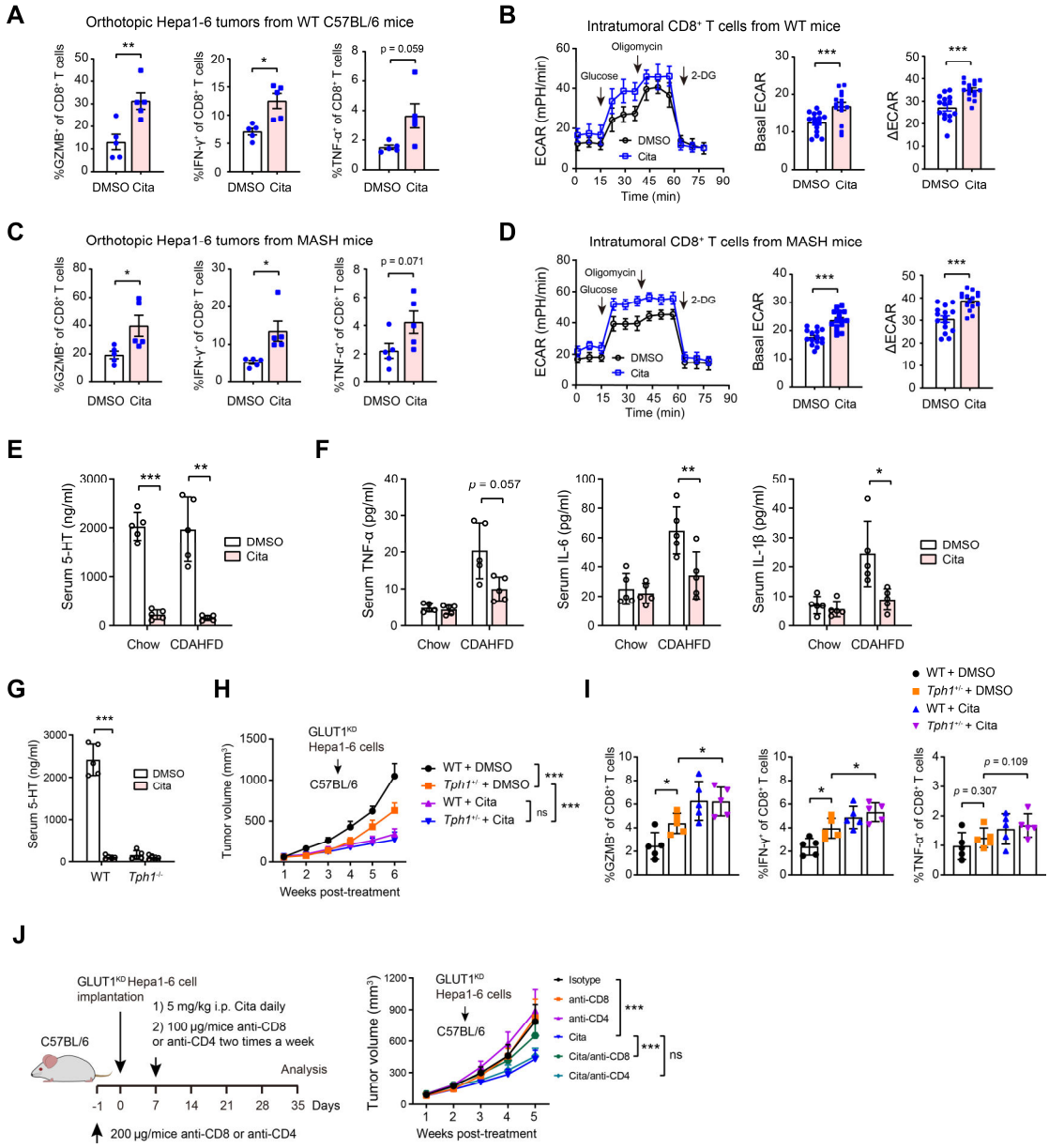

Figure 4. Citalopram activates CD8⁺ T cells.

(**A**, **B**) Measurement of CD8⁺ T cell function and glycolysis in orthotopic tumor tissues from WT C57BL/6 mice (n = 5 per group). (**C**, **D**) Measurement of CD8⁺ T cell function and glycolysis in orthotopic tumor tissues from MASH mice (n = 5 per group); Basal ECAR indicates glycolysis after the addition of glucose, and ΔECAR represents the difference between oligomycin-induced ECAR and 2-DG-induced ECAR. (**E**) Serum 5-HT levels in GLUT1^{KD} Hepa1-6 tumor-bearing mice fed with chow diet or CDAHFD, with the presence or absence of citalopram treatment (n = 5 per group). (**F**) Serum TNF-α, IL-1β, and IL-6 levels in GLUT1^{KD} Hepa1-6 tumor-bearing mice fed with chow diet or CDAHFD, with the presence or absence of citalopram treatment (n = 5 per group). (**G**) Serum 5-HT levels in WT C57BL/6

and *Tph1*$^{-/-}$ mice, with the presence or absence of citalopram treatment (n = 5 per group). (**H**) Tumor growth of WT and *Tph1*$^{-/-}$ mice after subcutaneous injection of Hepa1-6 cells and treatment with citalopram. (**I**) Measurement of CD8^{+} T cell function in tumor tissues from the groups mentioned in **H**. (**J**) The therapeutic effect of citalopram on GLUT1^{KD} Hepa1-6 tumor was tested in the presence or absence of CD4^{+} T or CD8^{+} T cell depletion. In all panels, *p < 0.05, **p < 0.01, ***p < 0.001; ns, non-significant. Values as mean ± SD and compared by the Student's t test (**A**-**G**), one-way ANOVA multiple comparisons with Tukey's method (**I**), and two-way ANOVA with Dunnett's multiple comparisons (**H**, **J**).

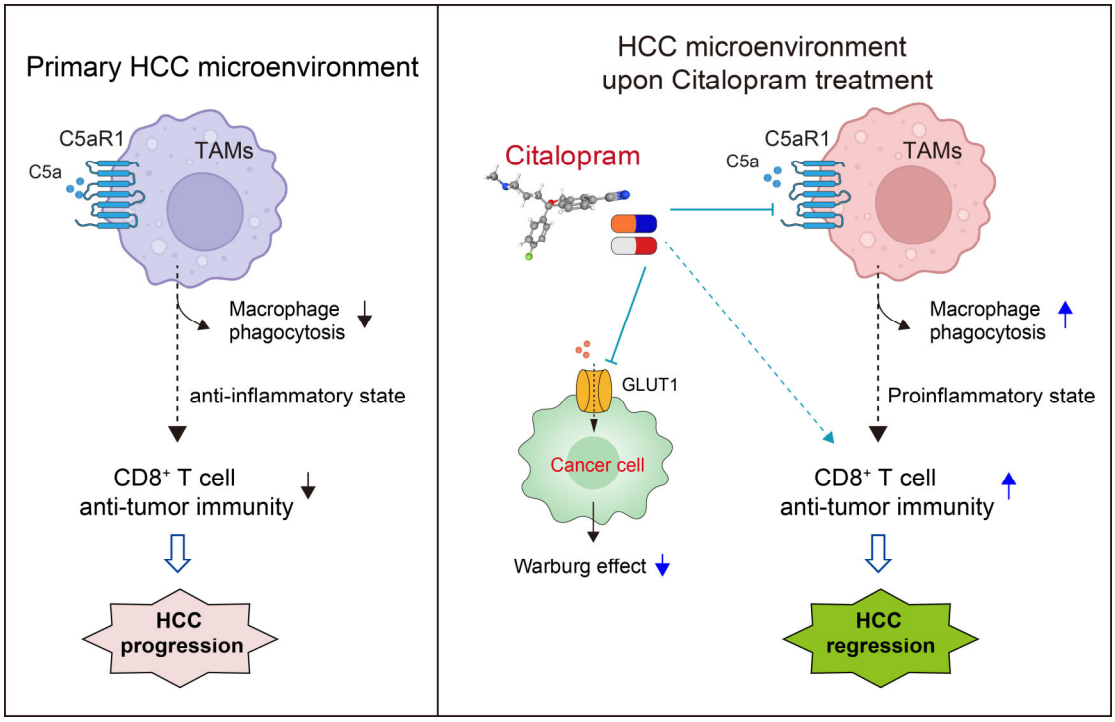

Figure 5. Mechanism model.

Model depicting the molecular mechanism by which citalopram inhibits the Warburg effect and promotes an anti-tumor response in hepatocellular carcinoma (HCC). In the primary HCC microenvironment (left panel), C5aR1-expressing tumor-associated macrophages (TAMs) exhibit reduced phagocytic capacity and an anti-inflammatory state, which correlates with diminished $CD8^+$ T cell anti-tumor immunity and HCC progression. Upon treatment with citalopram (right panel), the drug not only inhibits the glycolytic metabolism of cancer cells by targeting GLUT1 (Dong et al., 2024) but also acts on C5aR1 expressed by TAMs, thereby enhancing macrophage-driven anti-tumor immunity. Additionally, citalopram induces a systemic immunostimulatory effect on $CD8^+$ T cell functions through yet-to-be-identified serotonergic mechanisms. The dotted line indicates a causal relationship that has not been fully established through direct evidence. The figure was created with BioRender (www.bioRender.com).